Journal of Materials Chemistry A

Accepted Manuscript

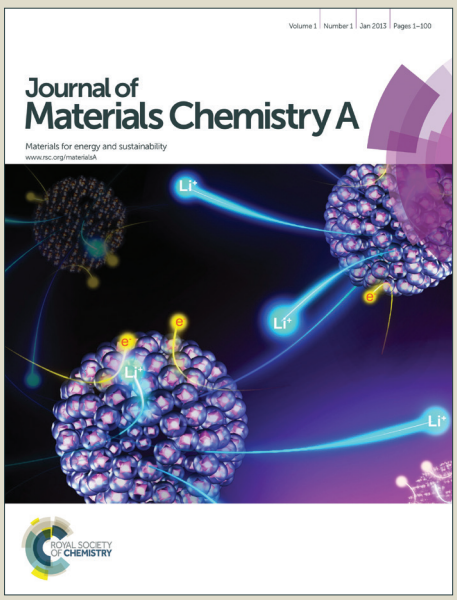

ROYAL SOCIETY OF CHEMISTRY

www.rsc.org/materialsA

Journal Name

RSCPublishing

COMMUNICATION

Facile one-pot synthesis of copper hexacyanoferrate nanoparticles functionalised silica monoliths for the selective entrapment of ^{137}Cs†

Cite this: DOI: 10.1039/x0xx00000x

Received 00th January 2012,
Accepted 00th January 2012

DOI: 10.1039/x0xx00000x

www.rsc.org/

Jérémy Causse*[a], Alexeï Tokarev[a], Johann Ravaux[a], Micheàl Moloney[a], Yves Barré[b] and Agnès Grandjean[a]

In this study, hexacyanoferrate nanoparticle (NP) functionalised silica monoliths were used to selectively remove Cs^+ from aqueous solutions which also contained large concentrations of Na^+. Various NP loading levels were examined from 0.2 %wt up to 5.1 %wt producing different ^{133}Cs and ^{137}Cs sorption results.

The goal of this study was to develop a facile synthetic route for the preparation of monolithic materials devoted to the decontamination of radioactive effluents. Here, the targeted radionuclide, ^{137}Cs, is one of the most problematic elements of the nuclear cycle. Radioactive ^{137}Cs is also widely present in contaminated liquid effluents from the Fukushima nuclear plant accident following the tsunami which occurred on March, 11th 2011 making ^{137}Cs extraction a topical issue[1]. Hexacyanoferrate (HCF) compounds from the Prussian Blue Analogue (PBA) family are very well known as selective Cs sorbents[2-6]. HCF compounds containing potassium in the lattice structures are quite efficient in the uptake of Cs ions; the exchange mechanism being the insertion of Cs ions into the structure, while K ions are concurrently released into solution[7]. These coordination polymers (HCF) are very selective towards Cs ions with regard to Na ions. However, due to their low mechanical hardness and their fine powder form leading to a slow filtration rate as well as a clogging problem, only small volumes of effluent can be treated. For this reason, the use of a bulk compound in column process decontamination cannot be considered, while monolithic materials with hierarchical porosity can.

In this study, the synthetic route used high internal phase emulsion (HIPE). This technique has been used by several teams in the past, in order to design organic[8, 9] or more recently inorganic macroporous monoliths[10-15]. In this latter case, the oil phase dispersed in the water phase acts as a soft template and allows the synthesis of macroporous monoliths after a washing treatment to remove the oil. The presence of surfactants in the procedure also ensures the final monolith to be mesoporous. In this paper, colloidal suspensions of HCF NPs dispersed into water make up the aqueous phase in a HIPE, which is then used to prepare the functionalised monolith materials in a one-pot procedure. The main advantage of this procedure is the absence of the impregnation step of the premade monoliths usually necessary to achieve functionalization[16]. Indeed, this step is usually long, requires the use of non-environmentally friendly solvents, and results in lower levels of incorporation. The first step of the procedure involves the preparation of colloidal suspension. In this study we prepared suspensions with two different copper hexacyanoferrate (CuHCF) concentrations; 9.0g/L (stoich.: $K_{1.77}Cu_{1.16}Fe(CN)_6$) and 32.2g/L (stoich.: $K_{2.05}Cu_{1.08}Fe(CN)_6$). This was done to allow an increase in the NP concentration incorporated into the final material without altering the volume of the aqueous phase. The large amount of water present in the structure of the NPs gave a stable colloidal suspension without the presence of a stabiliser. The NP synthetic procedure is explained in the ESI. The next step involves the preparation of the oil in water emulsion and the synthesis of the functionalised silica monolith itself (ESI). The color of the monoliths switches from white to light red / violet as the concentration of CuHCF NPs inside the monoliths is increased (ESI, S1).

Examination of the morphology of the microstructure showed that these monoliths are made of stacks of interconnected silica spheres with mean size around 8µm (ESI, S2). TEM observations have also been conducted on these monoliths (see Fig. 2, and ESI for experimental process). TEM showed that the porosity of the wall delimiting silica spheres possess local hexagonal organisation. However, this organisation was not homogeneous in the whole sample as proved by SAXS measurements which didn't exhibit more than the first correlation peak (ESI – S4).

TEM also showed that the CuHCF NPs were highly aggregated, and located in the silica walls. This location is due to the hydrophilicity of CuHCF NPs. As mentioned earlier CuHCF NPs are highly hydrophilic and they therefore remain in the HIPE water phase, and then are located in the silica wall after the silica polymerisation step. Indeed, large amounts of water are linked to the defects in the NPs crystalline lattice as shown by FT-IR spectra (ESI – S5) and previous work[17, 18].

.

Journal Name

RSCPublishing

COMMUNICATION

Table 1 Properties of CuHCF NPs functionalised monoliths.

Sample	0.2@SiO_2	0.4@SiO_2	0.8@SiO_2	1.8@SiO_2	2.9@SiO_2	5.1@SiO_2
CuHCF Coll. Susp. (g/l)	9.0	9.0	9.0	9.0	32.2	32.2
R[a]	0.07	0.11	0.24	0.64	0.24	0.64
[CuHCF] exp. (%wt)[b]	0.2	0.4	0.8	1.8	2.9	5.1
S_{BET} (m^2/g)/D_{BJH} (nm)	290/2.6	278/2.7	383/2.7	479/2.7	547/3.1	643/6.2
[CuHCF] th. (%wt)[c]	0.3	0.6	1.2	2.5	4.4	8.4
Yield NP (%)[d]	66.7	66.7	66.7	72.0	65.9	60.7

[a] Ratio of CuHCF colloidal suspension over to surfactant solution defined as $R = V_{coll.susp.}/V_{surfactant\ solution}$. [b] Given by ICP-AES measurements after monolith dissolution. [c] Given by calculation with regard to the total amount of colloidal suspension used in the synthesis procedure. [d] Ratio between experimental and theoretical concentration of CuHCF nanoparticles in the final monolith

These results differ from the well-known Pickering emulsion process also used for HIPE monolith synthesis where NPs go towards the oil water interface to stabilise emulsions[19, 20].This has been confirmed with interfacial tension measurements which show no drastic effect of CuHCF NPs on the dodecane/water interface. Therefore, most of CuHCF are in the water phase and only a few are located at the dodecane/water interface.

The main properties of the synthesised monoliths are presented in the Table 1. It is noteworthy that some NPs are lost during the solvent washing treatment with retention rates between 60.7% and 72.0%. In addition, the porous properties change gradually with the concentration of NPs entrapped in the material. It is clear therefore that the presence of CuHCF NPs plays a role on porous surface and mesopore size of monoliths. This effect will be discussed later in a future paper.

The Cs sorption results clearly show the efficiency of the functionalised monoliths (Fig. 1). These experiments were carried out by immersing a given mass (10mg) of each monolith in an aqueous solution (20mL) containing $CsNO_3$ (1.10^{-4} mol/L) and CH_3COONa (1.10^{-3} mol/L) in order to check the materials selectivity towards Cs. It was necessary to use Cs concentration above that of real world conditions (i.e. Fukushima rinse water) as to allow for detection with an ionic chromatography device. For each measurement, a certain mass of functionalised monolith was used to ensure that the sorption conditions were well above that of CuHCF NP saturation with Cs. The remaining Cs concentration after a 24 hours sorption was then measured. Past studies showed that this waiting time was long enough so that the sorption equilibrium was reached[21]. The total Cs entrapped in the monoliths is plotted in Fig. 1. The red data shows, as expected, that the higher the NP concentration inside the monoliths, the more Cs is extracted from aqueous solution, with sorption capacity up to 0.08 mmol per gram of monolith (i.e. 10.6mg of ^{133}Cs per gram of monolith). Secondly, by increasing the concentration of colloidal suspension used to prepare monoliths, we increased the amount of Cs extracted from the solutions. This effect is due to the higher stoichmetric potassium content within the crystalline structure of this batch of CuHCF.

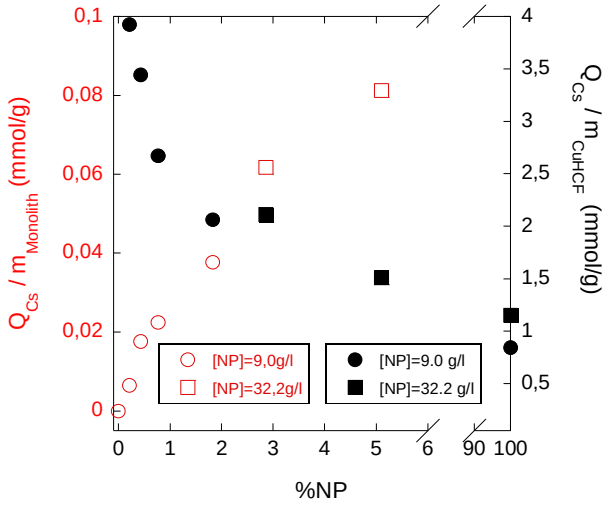

Fig. 1 Quantity of Cs adsorbed as a function of CuHCF NPs mass ratio in the monoliths. [NP] refers to concentration of NPs in the colloidal suspension used for the preparation of monoliths

The amount of Cs entrapped in the monolith normalised with regard to the total mass of NPs present in the monolith (Q_{Cs}/m_{CuHCF}) decreases as the NP concentration is increased. This continues with the value getting closer and closer to the value obtained for bulk CuHCF (powder of pure CuHCF, values at 100% NP). However, in all cases, this normalised capacity is always higher when functionalised monolith samples are used compared to the bulk material. This evolution shows that the lower the NP content the higher the normalised sorption capacities. We would argue that this is due to the NP aggregation effect within monoliths. As the concentration of NP increases so too does the degree of aggregation. This aggregation effect leads to a decrease in the surface area available. This nanoparticle aggregation has been observed, as already mentioned, by TEM (Fig. 2 and ESI for experimental procedure).

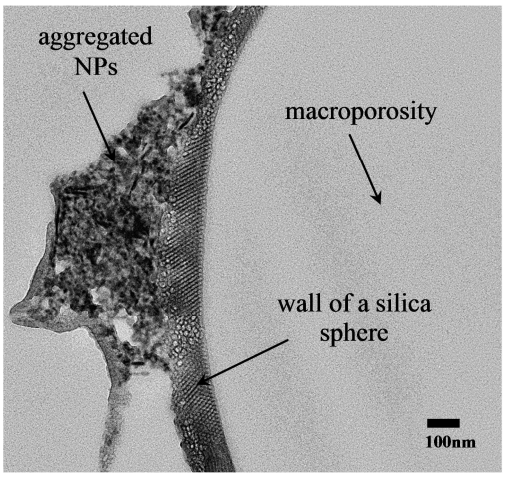

Fig. 2 TEM image of the monolith containing 5.1%wt of CuHCF NPs (5.10@SiO_2)

Table 2 shows results obtained with radioactive cesium. In this case, the distribution coefficient is used to assess selectivity of the materials towards ^{137}Cs. This value is noted K_d (ml/g) and is expressed as follows:

$$K_d = \frac{(A_0 - A_{eq})}{A_{eq}} \frac{V}{m_{CuHCF}} \quad (1)$$

where A_0 is the initial radioactivity, A_{eq} the radioactivity at equilibrium after sorption, V (ml) is the volume of the effluent used for the experiment and m_{CuHCF} (g) is the mass of CuHCF present in the solid sample. K_d^* is the distribution coefficient normalised with total mass of the materials (monolith or CuHCF in the case of bulk sample).

The initial solution activity was 41.2 kBq/L corresponding to Cesium concentrations of about 9.10^{-11}mol/L. In order to simulate unusual situations, such as contaminated seawater used to cool down damaged Fukushima reactors, the initial solution was enriched with salts (ESI).

Table 2 Distribution coefficients K_d and K_d^* for monolith and bulk materials

Sample	0.2@SiO_2	1.8@SiO_2	5.1@SiO_2	Bulk 32g/L
K_d^* (ml/g)	2.4 10^3	3.0 10^4	1.1 10^5	3.1 10^6
K_d (ml/g)	1.2 10^6	1.7 10^6	2.2 10^6	3.1 10^6

Table 2 shows K_d^* and K_d for 3 functionalised monoliths and bulk CuHCF. It is well known that the presence of sodium ions interfere with cesium sorption by PBA compounds[22]. However, in our case, even with concentrations of sodium and other cations far in excess of the Cs, the level of the distribution coefficients remains very high.

As expected, K_d^* values increase with CuHCF NPs ratio and finally reach 1.1 10^5 ml/g for the monolith loaded with 5.1 %wt of CuHCF NPs. This value can be compared to results obtained for other nanocomposites and radioactive cesium in past studies. Many authors used HCFs with various transition metals (Cu, Co, Zn, Ni) to functionalise organic (PAN, ion exchanger) or inorganic (powder, beads - SiO_2, ZrO_2, Al_2O_3, Fe_3O_4) supports. The values of K_d^* are found to be between 5.6 10^3 ml/g and 5 10^4 ml/g for solutions with lower activities (20 kBq/L, 10 kBq/L, 1.47 kBq/L)[18, 23-26]. To the best of our knowledge, only Delchet synthesised nanocomposites for ^{137}Cs with higher values of K_d^*, up to 8.10^5 mL/g[21]. However, experimental conditions were different with lower activity in the ^{137}Cs solution (20 kBq/L) and with a lower concentration of sodium ions (0.42 mol/L versus 0.65mol/L in our study). This is therefore quite hard to use as a true comparison. However, the values for K_d^* obtained with the monoliths developed in this work are competitive with regard to other studies carried out in the recent past. It should therefore be borne in mind that unlike previously mentioned materials, monolithic materials allow for a constant flow process on ^{137}Cs contaminated effluents to be performed.

Table 2 also shows high K_d (above 10^6 ml/g) for the three functionalised monoliths and bulk CuHCF material. However, the evolution of K_d differs from the results shown for non-radioactive Cesium in Fig. 1. This is due to the very low Cesium concentration in the case of radioactive effluents. Indeed, ^{137}Cs concentrations are so low (~10^{-11} mol/L) that the CuHCF NPs are very far from saturation. Therefore, the NPs aggregation observed inside the monoliths has no drastic effect in such conditions. While the K_d values should be identical for each of these samples, they are not. Table 2 shows a slight increase in the K_d values as NPs concentration in the monoliths increases. This could be due to a slight alteration of the NPs lattice structure due to the monoliths preparation experimental conditions. This alteration could slightly change selectivity of the monoliths towards ^{137}Cs and is therefore only noteworthy when Cs concentration is very weak. This effect also could be due to the greater accessibility for Cs to NPs surface caused by increased mesopore size for monoliths with high CuHCF NPs content, from 2.6nm for 0.2@SiO_2 to 6.2nm for 5.1@SiO_2 (Table 1). However, high K_d values obtained for all materials show good accessibility and selectivity of NPs for Cs ions even if NPs are located in silica walls with quite low mesopore sizes.

Conclusions

In summary, we prepared copper hexacyanoferrate nanoparticles functionalised monoliths suitable for aqueous wastes decontamination purposes. The original way of functionalisation described in this paper allowed us to synthesize monoliths with high levels of nanoparticles loading. Therefore, these materials present high cesium sorption capacity up to 10.6mg/g.

Finally sorption experiments using radioactive ^{137}Cs allowed us to show selectivity of the functionalised monolith even with huge concentrations of competitive cations such as sodium. This point is crucial in the field of highly saline wastewater decontamination such as in the case of Fukushima Daiichi rinse water treatment.

Acknowledgements

We thank the French Agency for Research (grant RSNR-Demeterres) for funding this work, Véronique Richard, Franck Godiard, Xavier Le Goff, Henri-Pierre Brau and Cyrielle Rey for TEM sample preparation and observations, and elemental analysis.

Notes and references

[a] *Institut de Chimie Séparative de Marcoule, ICSM, UMR 5257, CEA-CNRS-UM2-ENSCM, BP17171, 30207 Bagnols sur Cèze, France.*
Fax: +33 466 797 611; Tel:+33 466 397 421;
E-mail: jeremy.causse@cea.fr
[b] *CEA/DEN/DTCD/SPDE, Laboratoire des Procédés Supercritiques et de Décontamination, BP17171, 30207 Bagnols sur Cèze, France*
† Electronic Supplementary Information (ESI) available: [SAXS data, FT-IR data, TEM images, ESEM images]. See DOI: 10.1039/b000000x/

1. D. Klein and M. Corradini, *Fukushima Daiichi: ANS Comittee Report*, 2012.
2. S. Szoke, G. Patzay and L. Weiser, *Radiochim. Acta*, 2003, **91**, 229-232.
3. J. B. Ayers and W. H. Waggoner, *J. Inorg. Nuc. Chem.*, 1971, **33**, 721-733.
4. I. M. Ismail, M. R. El-Sourougy, N. A. Moneim and H. F. Aly, *J. Radioanal. Nucl. Chem.*, 1998, **237**, 97-102.
5. C. Loos-Neskovic, S. Ayrault, V. Badillo, B. Jimenez, E. Garnier, M. Fedoroff, D. J. Jones and B. Merinov, *J. Solid State Chem.*, 2004, **177**, 1817-1828.
6. T. Sangvanich, V. Sukwarotwat, R. J. Wiacek, R. M. Grudzien, G. E. Fryxell, R. S. Addleman, C. Timchalk and W. Yantasee, *J. Hazard. Mater.*, 2010, **182**, 225-231.
7. P. A. Haas, *Sep. Sci. Technol.*, 1993, **28**, 2479-2506.
8. P. Hainey, I. M. Huxham, B. Rowatt, D. C. Sherrington and L. Tetley, *Macromolecules*, 1991, **24**, 117-121.
9. N. R. Cameron, *Polymer*, 2005, **46**, 1439-1449.
10. A. Imhof and D. J. Pine, *Nature*, 1997, **389**, 948-951.
11. B. P. Binks, *Adv. Mater.*, 2002, **14**, 1824-1827.
12. F. Carn, A. Colin, M. F. Achard, H. Deleuze, E. Sellier, M. Birot and R. Backov, *J. Mater. Chem.*, 2004, **14**, 1370-1376.
13. J. G. Alauzun, S. Ungureanu, N. Brun, S. Bernard, P. Miele, R. Backov and C. Sanchez, *J. Mater. Chem.*, 2011, **21**, 14025-30.
14. N. Brun, S. R. S. Prabaharan, C. Surcin, M. Morcrette, H. Deleuze, M. Birot, O. Babot, M. F. Achard and R. Backov, *J. Phys. Chem. C*, 2012, **116**, 1408-1421.
15. S. Ungureanu, G. Sigaud, G. L. Vignoles, C. Lorrette, M. Birot, A. Derré, O. Babot, H. Deleuze, A. Soum, G. Pécastaings and R. Backov, *J. Mater. Chem.*, 2011, **21**, 14732-40.
16. N. Gartmann, C. Schütze, H. Ritter and D. Brühwiler, *The Journal of Physical Chemistry Letters*, 2010, **1**, 379-382.
17. S. Adak, L. L. Daemen, M. Hartl, D. Williams, J. Summerhill and H. Nakotte, *J. Solid State Chem.*, 2011, **184**, 2854-2861.
18. R. R. Sheha, *J. Coll. Int. Sci.*, 2012, **388**, 21-30.
19. R. Aveyard, B. P. Binks and J. H. Clint, *Adv. Coll. Int. Sci.*, 2003, **100-102**, 503-546.
20. N. Brun, S. Ungureanu, H. Deleuze and R. Backov, *Chem. Soc. Rev.*, 2011, **40**, 771-788.
21. C. Delchet, A. Tokarev, X. Dumail, G. Toquer, Y. Barre, Y. Guari, C. Guerin, J. Larionova and A. Grandjean, *RSC Adv.*, 2012, **2**, 5707-5716.
22. A. Nilchi, R. Saberi, M. Moradi, H. Azizpour and R. Zarghami, *Chem. Eng. J.*, 2011, **172**, 572-580.
23. T. P. Valsala, A. Joseph, J. G. Shah, K. Raj and V. Venugopal, *J. Nuc. Mater.*, 2009, **384**, 146-152.
24. R. Turgis, G. Arrachart, C. Delchet, C. Rey, Y. Barré, S. Pellet-Rostaing, Y. Guari, J. Larionova and A. Grandjean, *Chem. Mater.*, 2014, **25(21)**, 4447-4453.
25. V. V. Milyutin, S. V. Mikheev, V. M. Gelis and E. A. Kozlitin, *Radiochemistry*, 2009, **51**, 298-300.
26. S. Tsuruoka, B. Fugetsu, F. Khoerunnisa, D. Minami, K. Takeuchi, M. Fujishige, T. Hayashi, Y. A. Kim, K. C. Park, M. Asai, K. Kaneko and M. Endo, *Mater. Express*, 2013, **3**, 21-29.